

# Molecular oxygen adsorption and dissociation on $\text{Au}_{12}\text{M}$ clusters with $\text{M} = \text{Cu}, \text{Ag}$ or $\text{Ir}$

Laura M. Jiménez-Díaz and Luis A. Pérez<sup>a</sup>

Instituto de Física, Universidad Nacional Autónoma de México, Apartado Postal 20-364, 01000 Ciudad de México, Mexico

Received 2 August 2017 / Received in final form 5 December 2017

Published online 22 March 2018 – © EDP Sciences, Società Italiana di Fisica, Springer-Verlag 2018

**Abstract.** In this work, we present a density functional theory study of the structural and electronic properties of isolated neutral clusters of the type  $\text{Au}_{12}\text{M}$ , with  $\text{M} = \text{Cu}, \text{Ag}$ , or  $\text{Ir}$ . On the other hand, there is experimental evidence that gold-silver, gold-copper and gold-iridium nanoparticles have an enhanced catalytic activity for the CO oxidation reaction. In order to address these phenomena, we also performed density functional calculations of the adsorption and dissociation of  $\text{O}_2$  on these nanoparticles. Moreover, to understand the effects of Cu, Ag, and Ir impurity atoms on the dissociation of  $\text{O}_2$ , we also analyze this reaction in the corresponding pure gold cluster. The results indicate that the substitution of one gold atom in a  $\text{Au}_{13}$  cluster by Ag, Cu or Ir diminishes the activation energy barrier for the  $\text{O}_2$  dissociation by nearly 1 eV. This energy barrier is similar for  $\text{Au}_{12}\text{Ag}$  and  $\text{Au}_{12}\text{Cu}$ , whereas for  $\text{Au}_{12}\text{Ir}$  is even lower. These results suggest that the addition of other transition metal atoms to gold nanoclusters can enhance their catalytic activity towards the CO oxidation reaction, independently of the effect that the substrate could have on supported nanoclusters.

## 1 Introduction

It is well established that gold nanoclusters deposited onto metal oxide surfaces, such as  $\text{TiO}_2$ ,  $\text{Co}_3\text{O}_4$ ,  $\text{ZrO}_2$  and  $\text{NiO}$ , can catalyze several chemical reactions including the CO oxidation at ambient and sub-ambient temperatures [1–4]. However, small nanoclusters generally tend to coalesce into larger particles, due to their high surface energy, provoking a diminution of their catalytic activity with time. It has been considered that the aggregation of other metallic elements to gold nanocatalysts can lead to an enhancement of their catalytic performance by preventing the Au nanoclusters from sintering and also inducing a synergistic effect that could boost their catalytic activity for specific chemical reactions. For example, Okumura et al. aggregated iridium to gold catalysts and found an enhancement of their catalytic activity for some oxidative reactions that take place at high temperatures, such as the dioxin decomposition [5]. Other experimental studies also indicate that the incorporation of iridium into  $\text{Au}/\text{TiO}_2$  catalysts can prevent the sintering of the gold particles and increases their catalytic activity for CO oxidation [6]. Similarly, Bokhimi et al. observed as well an increment of the catalytic activity for the CO oxidation of the  $\text{Ir-Au}/\text{TiO}_2$  catalysts, in comparison with that of the  $\text{Au}/\text{TiO}_2$  ones [7]. The corresponding transmission electron microscopy analysis indicate that these  $\text{Ir-Au}/\text{TiO}_2$  catalysts comprise gold-iridium nanoparticles with sizes close to 1 nm

and, likely, these nanoclusters are the responsible of augmenting the CO oxidation catalytic activity. Similarly, for the CO oxidation reaction, it has been shown that gold-copper bimetallic nanoclusters deposited onto silicon dioxide have higher catalytic activities than monometallic gold catalysts [8]. Besides, for sub-ambient temperatures, even the addition of a small quantity of copper can produce a huge increment in the reaction rate. Furthermore,  $\text{Au-Cu}$  bimetallic nanoparticles supported on titania are temporally more stable [9,10] and can be even three times more active than  $\text{Au}/\text{TiO}_2$  for the CO oxidation reaction at 20 °C [10]. Likewise,  $\text{Au-Ag}/\text{TiO}_2$  not only catalyze the CO oxidation reaction at sub-ambient temperatures but also are temporally more stable than monometallic gold catalysts at 20 °C [11,12]. It is worth mentioning that changing the support from a reducible one, such as  $\text{TiO}_2$ , to nonreducible ones, such as silicas, practically does not alter the performance of the  $\text{Au-Ag}$  catalysts for the CO oxidation, suggesting that the entire reaction could mainly occur on the bimetallic nanoparticles [11,13].

Compared to monometallic catalysts, the better catalytic performance obtained when iridium, copper or silver atoms are aggregated to supported gold nanoclusters indicate that there could be a synergistic effect between gold and other transition metals in the catalysis of the CO oxidation reaction. On the other hand, due to the progress attained in the fabrication of controllable cluster sources, the investigation of the physical and chemical properties of isolated nanoclusters has become an intense field of research. Gas-phase metal clusters have been considered

<sup>a</sup> e-mail: lperez@fisica.unam.mx

as model systems that allow a deeper understanding of the energetics of catalytic reactions mediated by metals [14]. In particular, since the adsorption and dissociation of  $O_2$  is a key step for the oxidation of CO, this phenomenon has been addressed on gas-phase gold clusters [15]. For example, it has been theoretically found that anionic gas-phase  $Au_N$  ( $N \leq 8$ ) nanoclusters interact stronger with the molecular oxygen than their cationic and neutral counterparts, and they also present an odd-even behavior as a function of the number of gold atoms, where the maxima are observed for even- $N$   $Au_N O_2$ -complexes [15]. Moreover, the monoplatinum doping of  $Au_{25}(SR)_{18}$  ( $SR = C_2H_4Ph$ ,  $Ph = C_6H_5$ ) provokes drastic changes on its optical, electronic, and catalytic properties [16].

In this work we present a density functional theory study of the adsorption and dissociation of molecular oxygen on neutral gas phase  $Au_{13}$ ,  $Au_{12}Cu$ ,  $Au_{12}Ag$  and  $Au_{12}Ir$  clusters, in order to gain insight into the effects of Cu, Ag and Ir on the catalytic activity of gold nanoclusters. It is worth mentioning that in order to avoid peculiarities that could arise from the 2D nature of small gold nanoclusters, we have considered the  $Au_{13}$  since it is the smallest one where its 3D nature has been established by different groups [17–19], allowing the modeling of reactive sites in 3D particles within a reasonable computing time for the calculation of energy barriers.

## 2 Computational details

The first step in our study was to find a distribution of the lowest energy isomers of  $Au_{13}$  clusters. These were obtained by performing global optimizations with a generalized version of the genetic-symbiotic algorithm by Michaelian et al. [20,21] using the many-body Gupta potential [22] to represent the energy. The Gupta parameters for gold are the same used by Cleri and Rosato [22]. In order to obtain the lowest-energy structure, the thirty more relevant isomers of this distribution were selected as initial configurations for a further local structural relaxation with the quasi-Newton BFGS method using the forces obtained from a density functional calculation (DFT) as implemented in the QUANTUM ESPRESSO code [23]. Then, the lowest-energy configurations of  $Au_{12}M$  ( $M = Ag, Cu$  or  $Ir$ ) were obtained by replacing each of the 13 gold atoms in the most stable  $Au_{13}$  isomer previously found with an  $M$  atom, and performing quasi-Newton BFGS structural relaxations using DFT forces. The subsequent  $O_2$  adsorption and dissociation studies were also performed by using the DFT formalism and, in all cases, the  $Au_{12}MO_2$  complexes were let free to relax during the calculations.

All DFT calculations were carried out within the generalized gradient approximation (GGA) using the PBEsol [24] expression for exchange-correlation energies and the geometries were converged until the Hellman-Feynman forces were smaller than  $0.05 \text{ eV}/\text{\AA}$ . Single  $\Gamma$ -point, spin polarized DFT calculations were performed using a plane-wave basis with an energy cutoff of 100 Ry. The relative tolerance in the density matrix, taken as the SCF convergence criterion, was set to  $10^{-6} \text{ eV}$ . A cubic unit cell

**Table 1.** Bond lengths  $r_e$  (in  $\text{\AA}$ ) and dissociation energies  $D_0$  (in eV) for Au, Cu, Ag and Ir neutral dimers.

Dimer	DFT-PBEsol	Exp. [26]
$Au_2$	$D_0 = 2.157, r_e = 2.493$	$D_0 = 2.29 \pm 0.02, r_e = 2.47$
$Cu_2$	$D_0 = 2.079, r_e = 2.195$	$D_0 = 2.01 \pm 0.08, r_e = 2.22$
$Ag_2$	$D_0 = 1.608, r_e = 2.531$	$D_0 = 1.65 \pm 0.03, r_e = 2.53$
$Ir_2$	$D_0 = 4.254, r_e = 2.202$	$D_0 = 3.7 \pm 0.7, r_e = 2.23$

of  $17 \times 17 \times 17 \text{\AA}^3$  was sufficient to electronically isolate periodic images of the cluster. Scalar-relativistic ultrasoft pseudopotentials were taken from <http://www.quantum-espresso.org> where the valence-electron configurations considered were:  $5d^{10} 6s^1$  for Au,  $3d^{9.5} 4s^{1.5}$  for Cu,  $4d^{9.5} 5s^{1.5}$  for Ag,  $5d^7 6s^2$  for Ir and  $2p^4 2s^2$  for O.

In this work, we have employed the Perdew-Burke-Erzenhof generalized gradient approximation revised for solids (PBEsol) [24] since it has been used to correctly predict the 2D–3D structural transition for anionic gold clusters [25]. The latter work also pointed out that traditional generalized gradient functionals are biased in favor of 2D structures and suggested that density functionals yielding accurate jellium surface energies are more suitable for gold clusters. To further support the suitability of the chosen functional, basis sets and pseudopotentials, we compared the calculated bond lengths and dissociation energies of Au, Cu, Ag and Ir neutral dimers with the corresponding experimental values. The results are presented in Table 1.

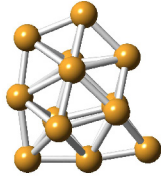
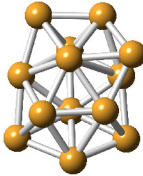
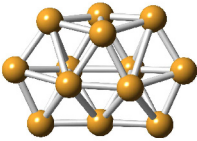
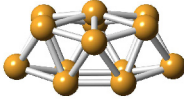
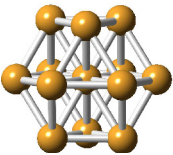
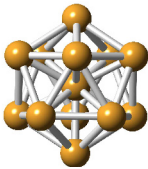
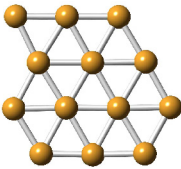
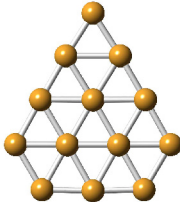
On the other hand, the energy barriers for  $O_2$  dissociation in the different  $Au_{12}M$  clusters were mapped by using the nudged elastic band method (NEB) [27] combined with the climbing image method (CI-NEB) [28]. In the process of NEB calculations seven images between the starting and ending geometries were used. The starting geometry was chosen as that where the molecular oxygen has the higher adsorption energy, whereas the final geometry corresponds to the nearby most stable configuration of the cluster with two dissociated oxygen atoms.

## 3 Results and discussion

The structure of the most stable isomer of  $Au_{13}$  has been subject of study during the last years. Although it has been theoretically established that the close-packed icosahedral and cuboctahedral geometries are not the lowest-energy isomers, several ab initio studies suggest that the lowest-energy isomer could be either 3D amorphous [17–19] or planar [29,30], where the energetic order seems to depend on the applied methodology, with plane-wave basis sets somewhat favoring two-dimensional structures [31]. More recently, by using two different methodologies [19,32], it has been found that the structure of the lowest-energy 3D isomer of  $Au_{13}$ , is the same as that found in this work.

The global optimizations of  $Au_{13}$  with the Gupta potential lead to an icosahedral structure as the global minimum, as found in previous works that also use semiempirical potentials [21,33]. However, after a DFT

**Table 2.** Lowest-energy structures of Au<sub>13</sub> and their energies relative to that of the most stable isomer (Isomer 1). BBP, cuboctahedral and icosahedral geometries are also shown for reference.

Isomer 1	Isomer 2	Isomer 3	BBP
			
0.000eV	0.050eV	0.070eV	0.280eV
Cuboctahedron	Icosahedron	Planar I	Planar II
			
0.96 eV	1.29eV	0.065eV	0.083eV

relaxation of the lowest-energy isomers obtained with the Gupta potential, the icosahedron is not the most stable one, in agreement with other studies [17–19,32]. Table 2 shows the three lowest-energy isomers of Au<sub>13</sub> obtained after the DFT-GGA structural relaxation of the 30 most stable Gupta isomers, together with the icosahedral and cuboctahedral geometries for reference. We also present the optimized structures of the buckled biplanar (BBP) cluster, which has been previously shown to be more stable than icosahedra, cuboctahedra and decahedra geometries [34,35], and two bidimensional structures reported in literature as the lowest-energy planar Au<sub>13</sub> clusters [29,30]. We observe that neither the planar structures nor the BBP cluster are the most stable ones, within the level of theory used in this work. It is worth to mention that Isomer 1 is also obtained as the lowest-energy 3D structure after a DFT-PBE geometry optimization, using the SIESTA code [36], among the 30 lowest-energy structures obtained with the genetic-symbiotic algorithm previously described. Isomers 1, 2 and 3 are nearly degenerated 3D structures where both 1 and 3 show prism-like motifs as described by Gruber et al. [31].

Table 3 shows the most stable configurations of the lowest-energy Au<sub>13</sub> structure with one gold atom replaced by M, with M=Cu, Ag or Ir, together with their corresponding binding energies per atom ( $E_b$ ).  $E_b$  is given by:

$$E_b = \frac{12E(\text{Au}) + E(\text{M}) - E(\text{Au}_{12}\text{M})}{13}, \quad (1)$$

where  $E(X)$  is the total energy of system  $X$ . Notice that the addition of one atom of Ag or Cu preserves the original

structure, whereas the addition of Ir distorts it. Compared to the pure gold cluster,  $E_b$  slightly diminishes when the silver atom is substituted and it increases when the impurities are copper or iridium.

Likewise, the first row of Table 4 shows the most stable configurations of O<sub>2</sub> adsorbed on the structures shown in Table 3, together with the corresponding O<sub>2</sub> adsorption energies ( $E_{\text{ads}}$ ), excess electronic charges ( $\Delta q$ ) on the O<sub>2</sub> molecule or in the molecule together with the doping atom ( $\Delta q^*$ ) and the O–O bond lengths ( $d_{\text{O–O}}$ ).  $E_{\text{ads}}$  is calculated from:

$$E_{\text{ads}} = E(\text{Au}_{12}\text{M}) + E(\text{O}_2) - E(\text{Au}_{12}\text{MO}_2), \quad (2)$$

where  $E(X)$  is the total energy of system  $X$ . Notice that the O<sub>2</sub> molecule always binds, in a staple configuration, to two atoms of the cluster where one impurity atom is involved. We obtained the following order for the adsorption energies  $E_{\text{ads}}(\text{Au}_{12}\text{AgO}_2) < E_{\text{ads}}(\text{Au}_{12}\text{CuO}_2) < E_{\text{ads}}(\text{Au}_{12}\text{IrO}_2)$ . We also calculated the excess of electronic charge ( $\Delta q$ ) on the O<sub>2</sub> molecule by using a Löwdin population analysis. For all the studied cases, there is charge transfer from the cluster to the adsorbed O<sub>2</sub> molecule, leading to a weakening of the O–O bond, being larger (around 1.3 Å) than the calculated value for the free O<sub>2</sub> molecule (1.215 Å). The charge excess on the adsorbed O<sub>2</sub> molecule indicates activation toward a peroxy-like state. Notice that, for the doped gold clusters, the Löwdin population analysis leads to a charge excess ( $\Delta q$ ) on the O<sub>2</sub> molecule that diminishes as the O–O bond length increases. However, this bond length does increase with the excess charge on the system formed by the O<sub>2</sub> molecule and the doping atom ( $\Delta q^*$ ).

**Table 3.** Lowest-energy structures of  $\text{Au}_{12}\text{Ag}$ ,  $\text{Au}_{12}\text{Cu}$  and  $\text{Au}_{12}\text{Ir}$ . Gold, silver, copper and iridium atoms are represented by yellow, gray, brown and blue spheres, respectively.

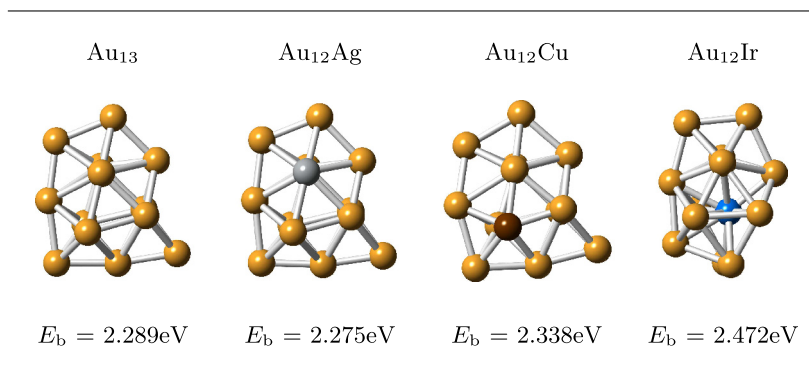
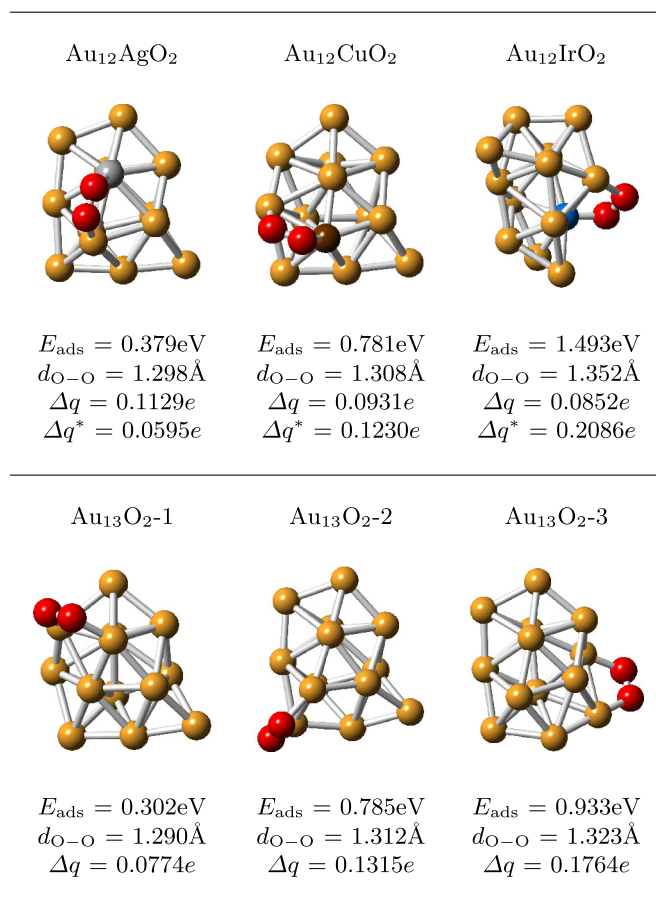


**Table 4.** Lowest-energy structures of  $\text{Au}_{12}\text{AgO}_2$ ,  $\text{Au}_{12}\text{CuO}_2$ ,  $\text{Au}_{12}\text{IrO}_2$  and  $\text{Au}_{13}\text{O}_2$  with the corresponding  $\text{O}_2$  adsorption energies ( $E_{\text{ads}}$ ), excess electronic charges ( $\Delta q$ ) on the  $\text{O}_2$  molecule or in the molecule together with the impurity atom ( $\Delta q^*$ ) and O–O bond lengths ( $d_{\text{O-O}}$ ).  $e$  denotes the electron charge. Gold, silver, copper, iridium and oxygen atoms are represented by yellow, gray, brown, blue and red spheres, respectively.



The second row of Table 4 shows the most stable configurations of the  $\text{O}_2$  molecule adsorbed on  $\text{Au}_{13}$  (Isomer 1), where the location of one of the gold atoms involved in the adsorption corresponds to that of the impurity atom of the  $\text{Au}_{12}\text{M}$  cluster shown above. The vertical comparison shows that the addition of iridium greatly enhances

the adsorption energy of  $\text{O}_2$ , the silver slightly augments this energy and the copper practically does not change it.

Figures 1a–1c show the calculated energy barriers for  $\text{O}_2$  dissociation on the studied  $\text{Au}_{12}\text{M}$  clusters, together with the corresponding initial, transition and final states. Likewise, Figures 1a'–1c' show the energy barriers for  $\text{O}_2$

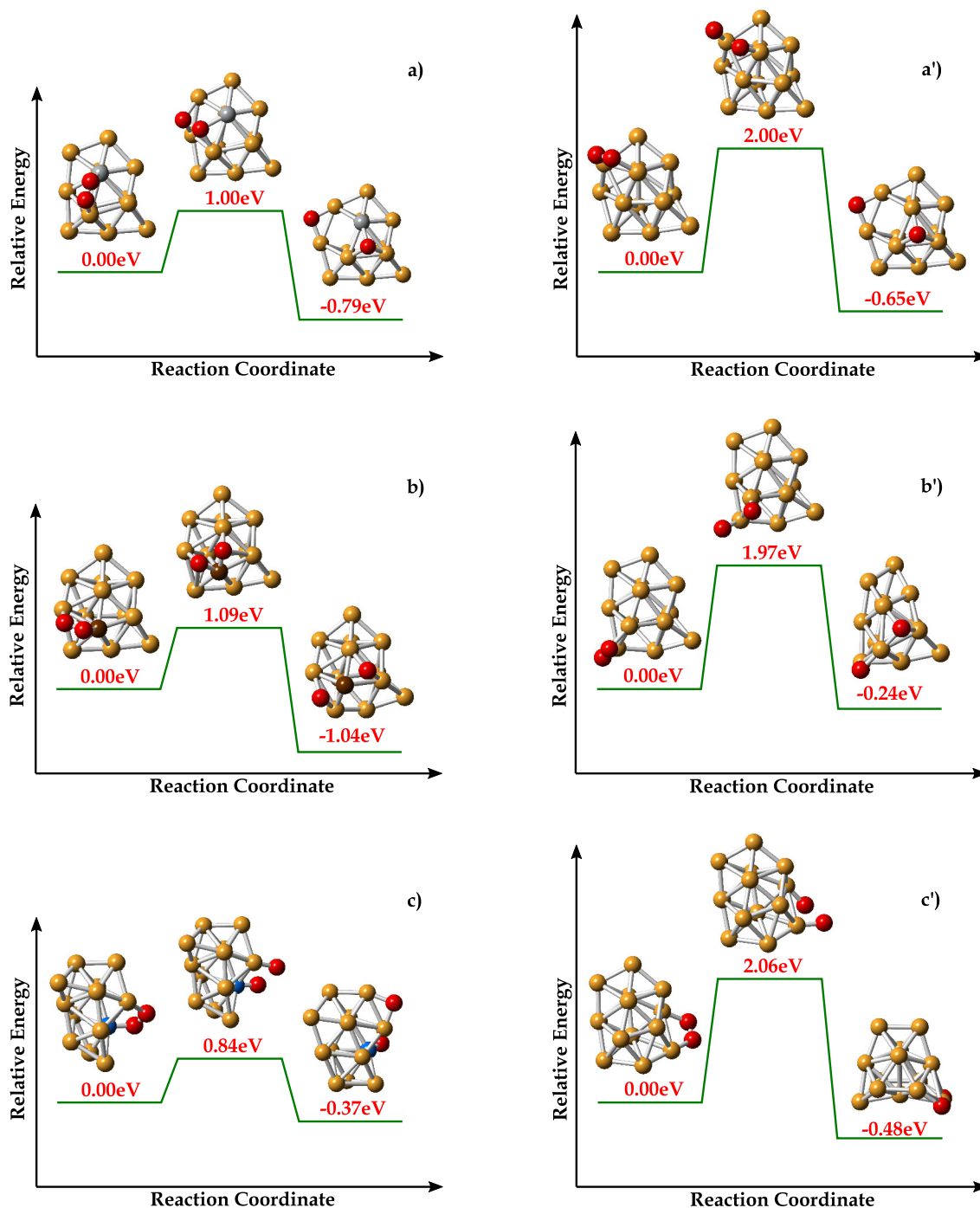


**Fig. 1.** Activation energy barriers for  $O_2$  dissociation on the lowest-energy isomers (a)  $Au_{12}Ag$ , (b)  $Au_{12}Cu$  and (c)  $Au_{12}Ir$  obtained from the most-stable  $Au_{13}$  cluster (Isomer 1 of Tab. 2), together with the geometries of the initial, transition and final states. Figures (a'), (b') and (c') show the activation energy barriers for  $O_2$  dissociation on Isomer 1 of  $Au_{13}$ , where the initial states correspond to those labeled as  $Au_{13}O_2$ -1,  $Au_{13}O_2$ -2, and  $Au_{13}O_2$ -3 in Table 4, respectively.

dissociation on the  $Au_{13}$  cluster, where the considered initial reaction site is the same as in the corresponding situation depicted in the left column. Notice that for gold clusters doped with Ag or Cu, we found that the most stable final state with the dissociated oxygen atoms also corresponds to the equivalent geometry for the pure  $Au_{13}$  case. However, for the  $Au_{12}Ir$  cluster, the location of the

dissociated oxygen atoms in the most stable final state is different in comparison with the pure gold cluster case. Moreover for cases (a), (b) and (a') the cluster geometry do not appreciably change between the initial and final states. For case (b') the cluster structure changes but it remains quite similar to the initial one. For cases (c) and (c') the cluster geometries of the final states appreciably

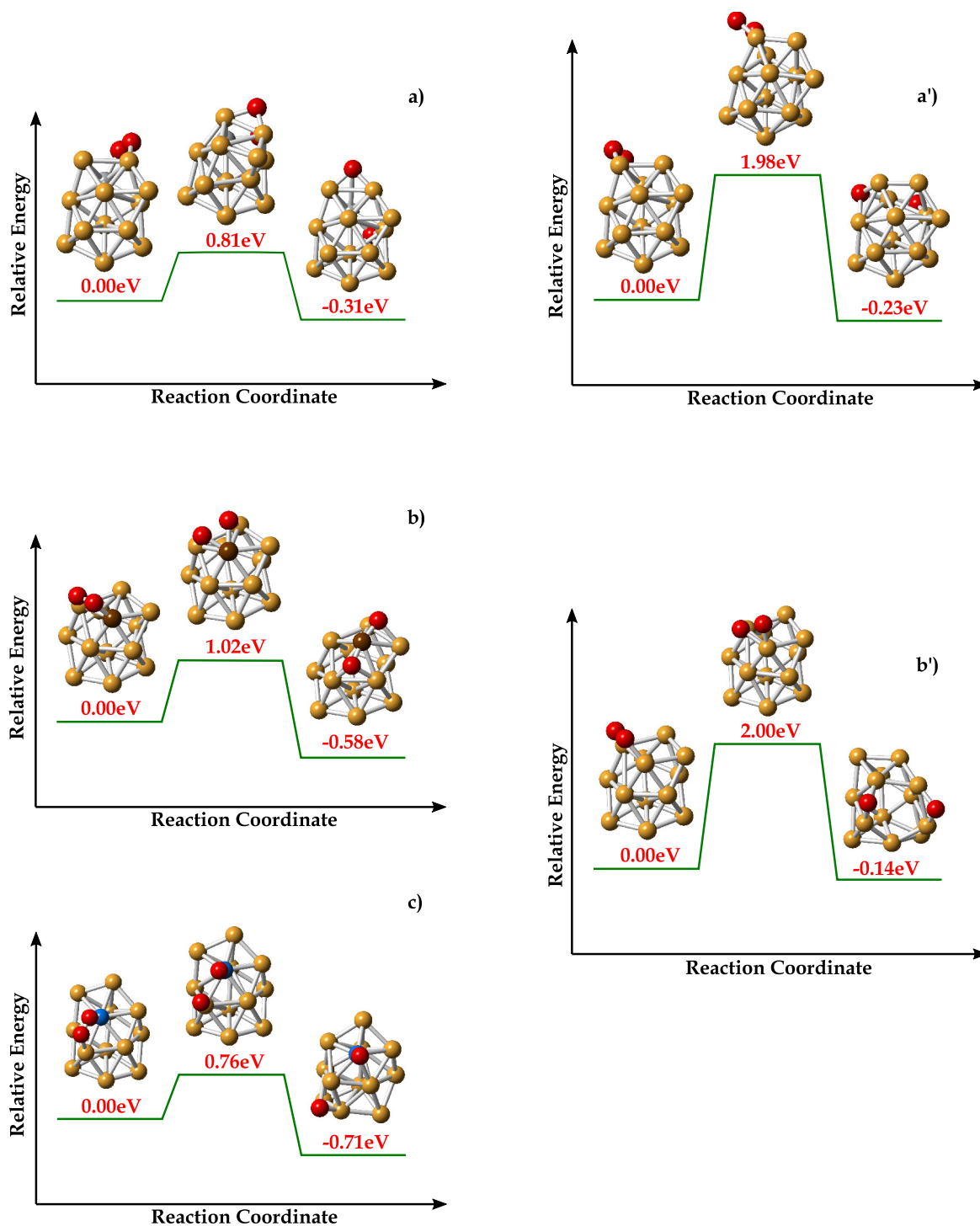


**Fig. 2.** Activation energy barriers for  $O_2$  dissociation on lowest-energy isomers (a)  $Au_{12}Ag$ , (b)  $Au_{12}Cu$  and (c)  $Au_{12}Ir$  obtained from the second most-stable  $Au_{13}$  isomer (Isomer 2 of Tab. 2), together with the geometries of the initial, transition and final states. Figures (a') and (b') show the activation energy barriers for  $O_2$  dissociation on Isomer 2 of  $Au_{13}$  for two different initial configurations.

differ from the corresponding initial ones. Notice that case (c') corresponds to the largest activation energy of the three  $Au_{13}$  cases considered.

Furthermore, for the three studied cases of  $O_2$  dissociation on Isomer 1 of  $Au_{13}$  cluster, the activation energies

slightly change with the location where the reaction occurs, and they are of the same order of magnitude ( $\sim 2\text{eV}$ ) than those previously reported for anionic  $Au_5$  gold clusters [15]. The addition of one atom of Cu, Ag or Ir diminishes these energies for nearly 1 eV. Moreover,

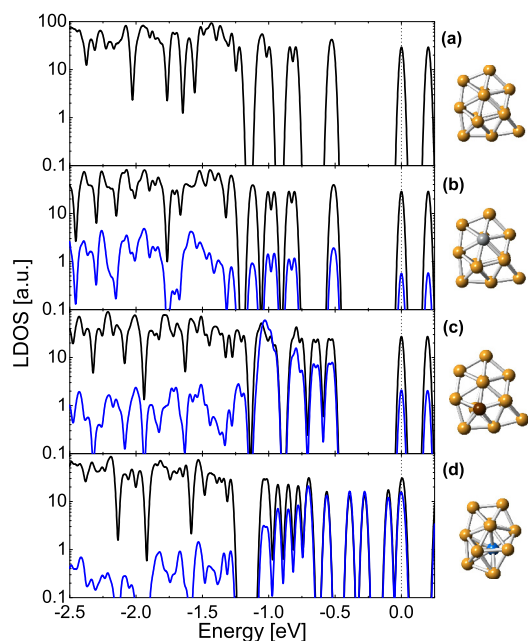


**Fig. 3.** Local densities of electronic states (LDOS) of the (a)  $\text{Au}_{13}$  (b)  $\text{Au}_{12}\text{Ag}$ , (c)  $\text{Au}_{12}\text{Cu}$ , and (d)  $\text{Au}_{12}\text{Ir}$  isomers shown in Table 3. The blue and black lines correspond to the density of states projected onto the M ( $M = \text{Ag}, \text{Cu}$  or  $\text{Ir}$ ) atom and the gold part of the cluster, respectively. The highest occupied molecular orbital (HOMO) of each system has been shifted to zero and indicated by a vertical dashed line. For clarity the vertical scale is logarithmic.

$\text{Au}_{12}\text{Cu}$  and  $\text{Au}_{12}\text{Ag}$  lead to similar activation energies ( $\sim 1$  eV), whereas the activation energy corresponding to the  $\text{Au}_{12}\text{Ir}$  cluster is even lower (0.84 eV). Observe that the activation energy barrier ( $E_{\text{act}}$ ) correlates with the corresponding adsorbed  $\text{O}_2$  bond length ( $d_{\text{O-O}}$ ), i.e., the larger  $d_{\text{O-O}}$  in the initial  $\text{Au}_{12}\text{MO}_2$  state corresponds to the lower  $E_{\text{act}}$ .

Figures 2a–2c show the calculated energy barriers for  $\text{O}_2$  dissociation on the lowest-energy isomers  $\text{Au}_{12}\text{M}$  obtained by using Isomer 2 of  $\text{Au}_{13}$  as parent structure, together with the corresponding initial, transition and final states. Similarly, Figures 2a' and 2b' show the energy barriers for  $\text{O}_2$  dissociation on Isomer 2 of  $\text{Au}_{13}$ . The initial reaction configuration in 2a' shares a common site with that depicted in 2a; whereas the initial reaction configuration in 2b' shares a common site with those shown in Figures 2b and 2c. Observe that the general trend previously found is conserved for Isomer 2 of  $\text{Au}_{13}$  and the  $\text{Au}_{12}\text{M}$  clusters derived from it. Namely, the substitution of one gold atom by a Cu, Ag or Ir atom lowers the activation energies barriers of the former pure gold cluster by nearly 1 eV.

The analysis of the local density of electronic states (LDOS) of the bare  $\text{Au}_{12}\text{M}$  clusters indicates, in this case, if the electronic states of the impurity atom ( $M = \text{Ag}, \text{Cu}$  or  $\text{Ir}$ ) are contributing to the total density of states (DOS) around the Fermi energy and then promoting their eventual interaction with the antibonding states of the oxygen molecule. An increase in the electron population

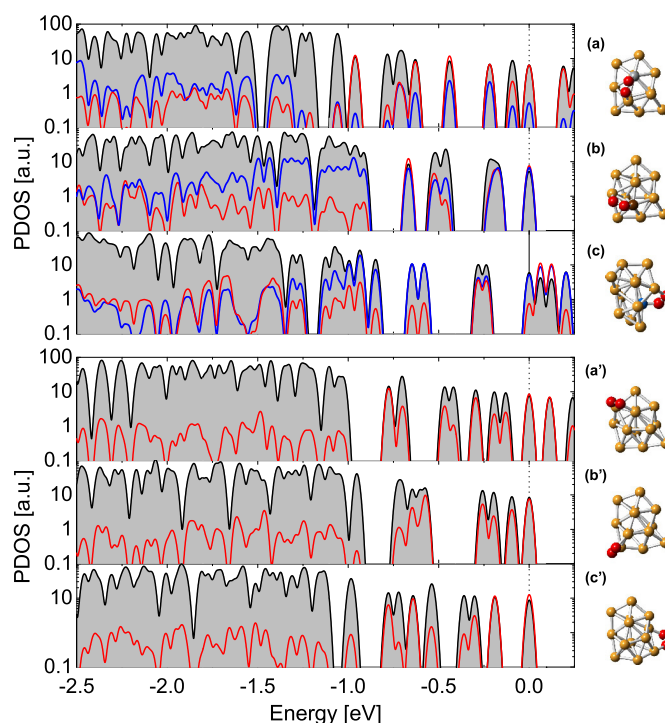


**Fig. 4.** Projected densities of electronic states (PDOS) of  $\text{Au}_{12}\text{MO}_2$  with (a)  $M = \text{Ag}$  (b)  $M = \text{Cu}$ , (c)  $M = \text{Ir}$  together with those corresponding to  $\text{Au}_{13}\text{O}_2$  in configurations (a') 1, (b') 2 and (c') 3 (see Tab. 4). Black, blue and red lines correspond to the PDOS of  $d$ -states of gold atoms,  $d$ -states of the M atom and  $p$ -states of oxygen atoms, respectively. The highest occupied molecular orbital (HOMO) of each system has been shifted to zero and indicated by a vertical dashed line. For clarity, the area below black lines has been shadowed and the vertical scale is logarithmic.

of the latter states upon cluster-molecule interaction leads to a weakening (or activation) of the O–O bond, as also indicated by the examination of the charge excess on the adsorbed  $\text{O}_2$  molecule. Figure 3 shows the density of states of the isomers  $\text{Au}_{12}\text{M}$  of Table 3 with (a)  $M = \text{Au}$ , (b)  $M = \text{Ag}$ , (c)  $M = \text{Cu}$  and (d)  $M = \text{Ir}$ , projected on the gold atoms (black lines) and on the M ( $M = \text{Ag}, \text{Cu}, \text{Ir}$ ) atom (blue lines). The vertical dashed lines indicate the position of the highest occupied molecular orbital (HOMO) of each cluster. Observe that there is hybridization between gold and M electronic states close to the HOMO, being stronger for the  $M = \text{Ir}$  case. Also notice that the substitution of one Au atom by Ag does not appreciably change the electronic spectra of the original  $\text{Au}_{13}$  cluster around the HOMO (Fig. 3b). On the other hand, the substitution of one Au atom by Cu leads to a cluster with different density of states (Fig. 3c), in spite of having almost the same structure. Finally, the electronic spectra of  $\text{Au}_{12}\text{Ir}$  and  $\text{Au}_{13}$  (Fig. 3c) are different between them due to the differences in both geometry and composition. Notice again that for the former cluster, the relative contribution of Ir to the DOS around the HOMO is much larger than that of Au atoms and then it is expected that this cluster could interact stronger with the oxygen molecule than the original  $\text{Au}_{13}$  one.

**Table 5.** O<sub>2</sub> adsorption energies ( $E_{\text{ads}}$ ), activation barriers ( $E_{\text{act}}$ ), O–O bond lengths ( $r_e$ ), excess electronic charges on the O<sub>2</sub> molecule ( $\Delta q$ ) or in the molecule together with the doping atom ( $\Delta q^*$ ), and the electron donation from the  $d$  orbitals of the M atom to the O<sub>2</sub> ( $\delta q_M^d$ ) for the Au<sub>13</sub>O<sub>2</sub> and Au<sub>12</sub>MO<sub>2</sub> (M = Ag, Cu, Ir) complexes depicted in Table 4.

	$E_{\text{ads}}$ (eV)	$E_{\text{act}}$ (eV)	$d_{\text{O-O}}$ (Å)	$\Delta q$ (e)	$\Delta q^*$ (e)	$\delta q_{\text{Au}}^d$ (e)	$\delta q_M^d$ (e)
Au <sub>12</sub> Ag	0.379	1.00	1.298	0.1129	0.0595	0.013	0.042
Au <sub>12</sub> Cu	0.781	1.09	1.308	0.0931	0.1230	0.011	0.110
Au <sub>12</sub> Ir	1.493	0.84	1.352	0.0852	0.2086	0.022	0.196
Au <sub>13</sub> -1	0.302	2.00	1.290	0.0774		0.023	
Au <sub>13</sub> -2	0.785	1.97	1.312	0.1315		0.023	
Au <sub>13</sub> -3	0.933	2.06	1.323	0.1764		0.021	

Likewise, Figure 4 shows the projected densities of electronic states (PDOS) of the six complexes Au<sub>12</sub>MO<sub>2</sub> depicted in Table 4 for gold  $d$  states (black lines), M (M = Ag, Cu, Ir)  $d$  states (blue lines) and oxygen  $p$  states (red lines). Upon adsorption of molecular O<sub>2</sub>, there is an ample and strong hybridization between the antibonding  $\pi^*$  orbitals of the oxygen molecule and the  $d$  orbitals of the cluster along intervals of 1.95 eV, 2.17 eV and 2.52 eV below the HOMO of the systems Au<sub>12</sub>MO<sub>2</sub> with M = Ag (Fig. 4a), M = Cu (Fig. 4b) and M = Ir (Fig. 4c), respectively. These values can be obtained by examining where the cumulative integral of the PDOS of O<sub>2</sub> reaches the value of ten electrons and realizing that the remaining electron population on O<sub>2</sub> resides in the now hybridized antibonding  $\pi^*$  states. Similarly, for the three Au<sub>13</sub>O<sub>2</sub>- $i$  ( $i = 1, 2, 3$ ) adsorption cases, the intervals where a strong hybridization between the former antibonding oxygen electronic states and the cluster electronic states are 2.27 eV ( $i = 1$ ), 2.26 eV ( $i = 2$ ) and 2.16 eV ( $i = 3$ ) below the cluster HOMO. Moreover, the relative contribution of the Ag  $d$  states to the HOMO of the Au<sub>12</sub>AgO<sub>2</sub> complex is similar to that of the Au  $d$  states and lower to that of the O  $p$  states. On the other hand, the relative contribution of the  $d$  states of Cu to the HOMO of the Au<sub>12</sub>CuO<sub>2</sub> complex is larger than that of Au  $d$  states and O  $p$  states. Likewise, the relative contribution of the Ir  $d$  states to the DOS at the HOMO of the Au<sub>12</sub>IrO<sub>2</sub> complex largely exceeds that of Au  $d$  states and O  $p$  states. Although not shown in Figure 4, it is worth mentioning that at the HOMO of all depicted systems, the contribution of the  $s$  orbitals of gold to the DOS is similar to that of their  $d$  orbitals. On the other hand, we also calculated the cumulative integrals up to the HOMO of both the M and gold densities of electronic states projected on the  $d$  orbitals before and after the O<sub>2</sub> adsorption, for each of the systems shown in Table 4. The differences between the integrals corresponding to the former and latter configurations indicate that there is an electron donation from the  $d$  orbitals of the cluster to the antibonding states of O<sub>2</sub>. A similar analysis shows that there is a weaker electron transfer from the O<sub>2</sub> electronic states to the  $s$  orbitals of the cluster. We also observe that the electron transfer from the  $d$  orbitals of the M atom (M = Ag, Cu, Ir) to the O<sub>2</sub> is always larger than the corresponding electron donation per atom of the  $d$  orbitals of gold atoms, for all the six cases depicted in Table 4. Furthermore, these electron donations from the  $d$  orbitals of the M atoms ( $\delta q_M^d$ ) to the

O<sub>2</sub> satisfy  $\delta q_{\text{Au}}^d < \delta q_{\text{Ag}}^d < \delta q_{\text{Cu}}^d < \delta q_{\text{Ir}}^d$ , where  $\delta q_{\text{Au}}^d$  is the average electron donation from the  $d$  orbitals of the gold part of the cluster to the O<sub>2</sub>. All the calculated values of  $\delta q_{\text{Au}}^d$  for the six complexes shown in Table 4 satisfy the previous inequality (see Tab. 5).

Finally, Table 5 summarizes the main results obtained in this work for the lowest-energy Au<sub>13</sub> isomer and the corresponding most stable Au<sub>12</sub>M (M = Ag, Cu, Ir) clusters obtained from it.

## 4 Conclusions

In this work, the structural and electronic properties of isolated neutral clusters of the type Au<sub>12</sub>M, with M = Cu, Ag, Ir or Au, as well as the adsorption of O<sub>2</sub> on these nanoparticles, were studied within the DFT-GGA framework. Moreover, the dissociation of O<sub>2</sub> on these nanoclusters was addressed by using NEB calculations. The substitution of an Au atom by Ag, practically does not change neither the geometry nor the electronic density of states (DOS) of the former Au<sub>13</sub> cluster, whereas the substitution of Au by Cu only changes the DOS but the geometry remains quite similar. Furthermore, the replacement of an Au atom by Ir leads to changes in both the geometry and the DOS of the former Au<sub>13</sub> cluster. On the other hand, for the Au<sub>13</sub> cluster, the O<sub>2</sub> adsorption energy strongly depends on the adsorption site, but the activation energy for the O<sub>2</sub> dissociation is nearly independent of it. The substitution of one gold atom in the Au<sub>13</sub> cluster by Ag, Cu or Ir diminishes this energy barrier by nearly 1 eV. The activation energies are similar for Au<sub>12</sub>Ag and Au<sub>12</sub>Cu, whereas it is lower for the Au<sub>12</sub>Ir case, where the relative contribution of the Ir to the DOS at the HOMO is much larger than those corresponding to O and Au. A detailed analysis of the densities of electronic states reveals that, upon O<sub>2</sub> adsorption, there is a large electron donation from the  $d$ -orbitals of the cluster to the antibonding states of oxygen and a weaker electron transfer from the latter states to the  $s$ -orbitals of the cluster. Moreover, the electron donation from the  $d$ -orbitals of the M atom (M = Ag, Cu, Ir) is larger than the average one of the gold atoms for all the studied clusters.

This theoretical study suggests that the addition of other transition metal atoms to gold nanoclusters can enhance their catalytic activity towards the CO oxidation reaction, independently of the effect that the substrate



could have on supported clusters, in agreement with previous experimental studies [11].

Finally, it should be pointed out that we only considered the effect of impurity atoms on the O<sub>2</sub> activation energy barrier in comparison to that corresponding to a pure gold cluster of the same size. Since the diminution in the energy barrier can be attributed to the impurity atom and then it is a local phenomenon, we expect that this trend should not critically depend on the cluster size. However, the particular value of the energy barrier could depend on it. This study will be addressed in a future work.

This work was supported by UNAM-DGAPA-PAPIIT under Grant IN107717. L.M.J.-D. acknowledges CONACyT scholarship. L.A.P. acknowledges partial support from “Cátedra Marcos Moshinsky” and PIIF No. 03. Computations were performed at Miztli of DGTIC-UNAM.

## Author contribution statement

Both authors contributed equally to this work.

## References

1. M. Haruta, T. Kobayashi, H. Sano, N. Yamada, *Chem. Lett.* **16**, 405 (1987)
2. M. Valden, X. Lai, D.W. Goodman, *Science* **281**, 1647 (1998)
3. M. Haruta, T. Kobayashi, S. Iijima, *J. Catal.* **115**, 301 (1989)
4. A. Knell, P. Barnickel, A. Baiker, A. Wokaun, *J. Catal.* **137**, 306 (1992)
5. M. Okumura, T. Akita, M. Haruta, X. Wang, O. Kajikawa, O. Okada, *Appl. Catal. B* **41**, 43 (2003)
6. A. Gómez-Cortés, G. Díaz, R. Zanella, H. Ramírez, P. Santiago, J.M. Saniger, *J. Phys. Chem. C* **113**, 9710 (2009)
7. X. Bokhimi, R. Zanella, C. Angeles-Chávez, *J. Phys. Chem. C* **114**, 14101 (2010)
8. X. Liu, A. Wang, T. Zhang, D.S. Su, C.Y. Mou, *Catal. Today* **160**, 103 (2011)
9. L. Li, C. Wang, X. Ma, Z. Yang, X. Lu, *Chin. J. Catal.* **33**, 1778 (2012)
10. A. Sandoval, C. Louis, R. Zanella, *Appl. Catal. B* **140–141**, 363 (2013)
11. A. Sandoval, A. Aguilar, C. Louis, A. Traverse, R. Zanella, *J. Catal.* **281**, 40 (2011)
12. X. Bokhimi, R. Zanella, V. Maturano, A. Morales, *Mater. Chem. Phys.* **138**, 490 (2013)
13. A.Q. Wang, J.H. Liu, S.D. Lin, T.S. Lin, C.Y. Mou, *J. Catal.* **283**, 186 (2005)
14. S.M. Lang, T.M. Bernhardt, *Phys. Chem. Chem. Phys.* **14**, 9255 (2012)
15. B. Yoon, H. Hakkinen, U. Landman, *J. Phys. Chem. A* **107**, 4066 (2003)
16. H. Qian, D.E. Jiang, G. Li, C. Gayathri, A. Das, R.R. Gil, R. Jin, *J. Am. Chem. Soc.* **134**, 16159 (2012)
17. J. Wang, G. Wang, J. Zhao, *Phys. Rev. B* **66**, 035418 (2002)
18. E.M. Fernández, J.M. Soler, I.L. Garzón, L.C. Balbás, *Phys. Rev. B* **70**, 165403 (2004)
19. J. Sun, X. Xie, B. Cao, H. Duan, *Comput. Theor. Chem.* **1107**, 127 (2017)
20. K. Michaelian, *Chem. Phys. Lett.* **293**, 202 (1998)
21. K. Michaelian, N. Rendón, I.L. Garzón, *Phys. Rev. B* **60**, 2000 (1999)
22. F. Cleri, V. Rosato, *Phys. Rev. B* **48**, 22 (1993)
23. P. Giannozzi et al., *J. Phys.: Condens. Matter* **21**, 395502 (2009)
24. J.P. Perdew, A. Ruzsinszky, G.I. Csonka, O.A. Vydrov, G.E. Scuseria, L.A. Constantin, X. Zhou, K. Burke, *Phys. Rev. Lett.* **100**, 136406 (2008)
25. M.P. Johansson, A. Lechtken, D. Schooss, M.M. Kappes, F. Furche, *Phys. Rev. A* **77**, 053202 (2008)
26. M.D. Morse, *Chem. Rev.* **86**, 1049 (1986)
27. G. Henkelman, G. Jóhannesson, H. Jónsson, in *Theoretical methods in condensed phase chemistry*, edited by S.D. Schwartz (Springer, Dordrecht, 2002), pp. 269–302
28. G. Henkelman, B.P. Uberuaga, H. Jónsson, *J. Chem. Phys.* **113**, 9901 (2000)
29. H. Sekhar De, S. Krishnamurthy, S. Pal, *J. Phys. Chem. C* **114**, 6690 (2010)
30. G. Zanti, D. Peeters, *Theor. Chem. Acc.* **132**, 1300 (2012)
31. M. Gruber, G. Heimel, L. Romaner, J.L. Brédas, E. Zojer, *Phys. Rev. B* **77**, 165411 (2008)
32. M. Amft, B. Johansson, N.V. Skorodumova, *J. Chem. Phys.* **136**, 024312 (2012)
33. J.P.K. Doye, D.J. Wales, *New J. Chem.* **22**, 733 (1998)
34. C.M. Chang, M.Y. Chou, *Phys. Rev. Lett.* **93**, 133401 (2004)
35. R.C. Longo, L.J. Gallego, *Phys. Rev. B* **74**, 193409 (2006)
36. J.M. Soler, E. Artacho, J.D.G. Gale, A. García, J. Junquera, P. Ordejón, D. Sánchez-Portal, *J. Phys.: Condens. Matter* **14**, 2745 (2002)